Semiconductors, 2022, Vol. 56, No. 14

Structural and photoelectric properties the thin film ZnO on $LiTaO_3$ substrate

© L.V. Grigoryev[1,2], A.A. Semenov[2], A.V. Mikhailov[3]

[1] St. Petersburg State University,
199034 St. Petersburg, Russia
[2] St. Petersburg State Electrotechnical University „LETI",
197022 St. Petersburg, Russia
[3] Vavilov State Optical Institute,
199054 St. Petersburg, Russia

E-mail: lvgrigoryev@mail.ru

Received July 27, 2021
Revised August 2, 2021
Accepted August 2, 2021

The results of the study of the structural and photoelectric properties of the $ZnO-LiTaO_3$ thin-film structure are presented. The results X-ray structural analysis and results atomic-force microscopy of the surface zinc oxide thin films synthesized on a single-crystal lithium tantalite substrate and on a KU-1 quartz substrate are presented. The spectral dependence of photoconductivity in the thin film structure of $ZnO-LiTaO_3$ and the structure of ZnO−quartz in the ultraviolet and visible spectral ranges are presented.

Keywords: zinc oxide, laser ablation, ferroelectric materials, X-ray structural analysis, atomic-force microscopy surface, photoconductivity, method Tikhonov-Lavrentiev regularization.

DOI: 10.21883/SC.2022.14.53860.9724

1. Introduction

Thin-film semiconductor–ferroelectric structures currently attract much research attention due to their potential applications in the design of microwave photonic, photoelectronic, acoustoelectronic, optoacoustic, and functional devices [1–3]. Thin films of piezoelectric semiconductors, such as ZnO, CdS, and AlN, are considered to be promising semiconductor materials for such devices. Zinc oxide (ZnO) films belong to the class of wide- and direct-bandgap semiconducting materials and, owing to low optical losses and a large bandgap width (~ 3.3 eV at room temperature), are used widely as active materials in photonic and microelectronic microdevices operating in the ultraviolet and visible spectral ranges [4,5].

Within this context, $ZnO-LiTaO_3$ provides an opportunity to construct optically or electrically controlled structures with the topology of a field-effect transistor or a photoconductive sensor with field control [6]. A comprehensive study of the structural and photovoltaic properties of thin films of zinc oxide as part of a piezoelectric semiconductor−ferroelectric structure needs to be performed in order to construct such microdevices. This article is a continuation of a series of research papers focused on the ZnO−ferroelectric structure [7–9].

The results of examination of the structural and photovoltaic properties of thin films of zinc oxide in thin-film ZnO−lithium tantalate ($ZnO-LiTaO_3$) and ZnO−quartz ($ZnO-SiO_2$) structures are reported below.

2. Sample preparation

Thin-film structures were created by laser ablation of a target made of pressed extra-pure grade ZnO powder [10–12]. Structures consisting of a thin ZnO film deposited onto a quartz substrate ($ZnO-SiO_2$) were fabricated on the surface of KU-1 quartz wafers. All substrates used in the study were polished to class 14. The synthesis of thin ZnO films by laser ablation was performed in a pulsed mode. The laser beam was scanned over the target surface in the process of deposition to prevent melting of the target of compressed ZnO powder and the accompanying splashing of large molten droplets onto the substrate and to exclude the possibility of burning of the target. The working volume of the stainless-steel reactor, which was used to synthesize zinc oxide films, was evacuated to a residual pressure below 0.01 Pa with a two-loop oil-free pumping system. A pulsed DPSS Nd : YAG laser operating at the fundamental wavelength of 1064 nm was used to perform pulsed laser ablation. The DPSS laser was operated in the giant-pulse mode. These pulses were generated using a cavity of an industrial laser modified to include an intracavity electrooptic modulator. The laser pulse repetition rate could be adjusted from 70 to 20 Hz in the film deposition process. The laser pulse energy was 640 mJ. The laser pulse duration was 10−12 ns. The collimated laser flux was introduced into the reaction chamber through a sapphire window. Laser radiation was focused onto the ZnO target surface to a spot with a diameter no greater than 540 μm. The distribution of laser radiation power over the beam section was Gaussian. The temperature of the

substrate made of lithium tantalate or quartz was measured with a thermocouple. Depending on the deposition mode, the substrate temperature varied from room temperature to 250°C. This ensured the preservation of the ferroelectric phase in the single-crystal lithium tantalate substrate. The ferroelectric substrate was heated by illuminating it with an IR lamp. The ZnO film thickness was monitored with a quartz microbalance in the process of its growth on the substrate.

Two types of samples were synthesized: square ZnO regions with a side length of 25 mm were prepared for structural studies, and strips 1.5 mm in width, 5 mm in length, and 3.0 μm in thickness were formed for the examination of photovoltaic properties.

3. Experimental results

X-ray diffraction studies of zinc oxide films were carried with a DRON-3M diffractometer. CuK_α radiation with a wavelength of 1.5418 AA was used.

The comparison of diffraction patterns of zinc oxide on quartz, zinc oxide on a lithium tantalate substrate heated to 250°C, and zinc oxide on a lithium tantalate substrate without preheating is presented in Figs. 1, *a–c*. According to the X-ray diffraction analysis data, all synthesized films have a nanocrystalline structure. The dimensions of ZnO crystals in the bulk of a thin zinc oxide film (in the $ZnO-LiTaO_3$ structure) calculated by the Selyakov–Scherrer formula [13] did not exceed 16 nm, and the dimensions of nanocrystals in a ZnO layer deposited on a quartz substrate did not exceed 12 nm.

The X-ray diffraction patterns of all the synthesized zinc oxide films contain a high-intensity diffraction maximum of hexagonal ZnO(002). Therefore, it is fair to state that films synthesized by pulsed laser ablation are characterized by a high degree of structural perfection. In addition, the presence of preferred axial texture in the *c* axis direction (perpendicular to the substrate surface) should be noted. Comparing the positions of diffraction peaks for zinc oxide films synthesized on a lithium tantalate substrate with preheating (Fig. 1, *b*) and on a quartz substrate (Fig. 1, *a*), we find that the intensity of peak (100) decreases from 0.8 to 0.33. The unchanged angular position of peaks (100) and (002) indicates that a zinc oxide film synthesized on a heated lithium tantalate substrate is not subjected to compression or stretching. The diffraction patterns (see Figs. 1, *b* and *c*) for ZnO films formed on hot or cold ferroelectric substrates contain reflections (101), (110), which are not found in the diffraction pattern for a zinc oxide film formed on a quartz wafer surface. A very weak reflection (102) at an angle around 48° is present in the diffraction patterns of all the studied films. The intensity of this reflection does not depend on the type of substrate used or the substrate temperature. It should be noted that the intensity of reflection (100) for a film synthesized on a $LiTaO_3$ substrate without preheating decreased by 13% relative to the intensity of similar peaks (reflections) in the diffraction patterns of films synthesized on a preheated $LiTaO_3$ substrate and decreased by 57% relative to the intensity of this reflection for films formed on a quartz substrate. At the same time, the intensity of peak (002) in

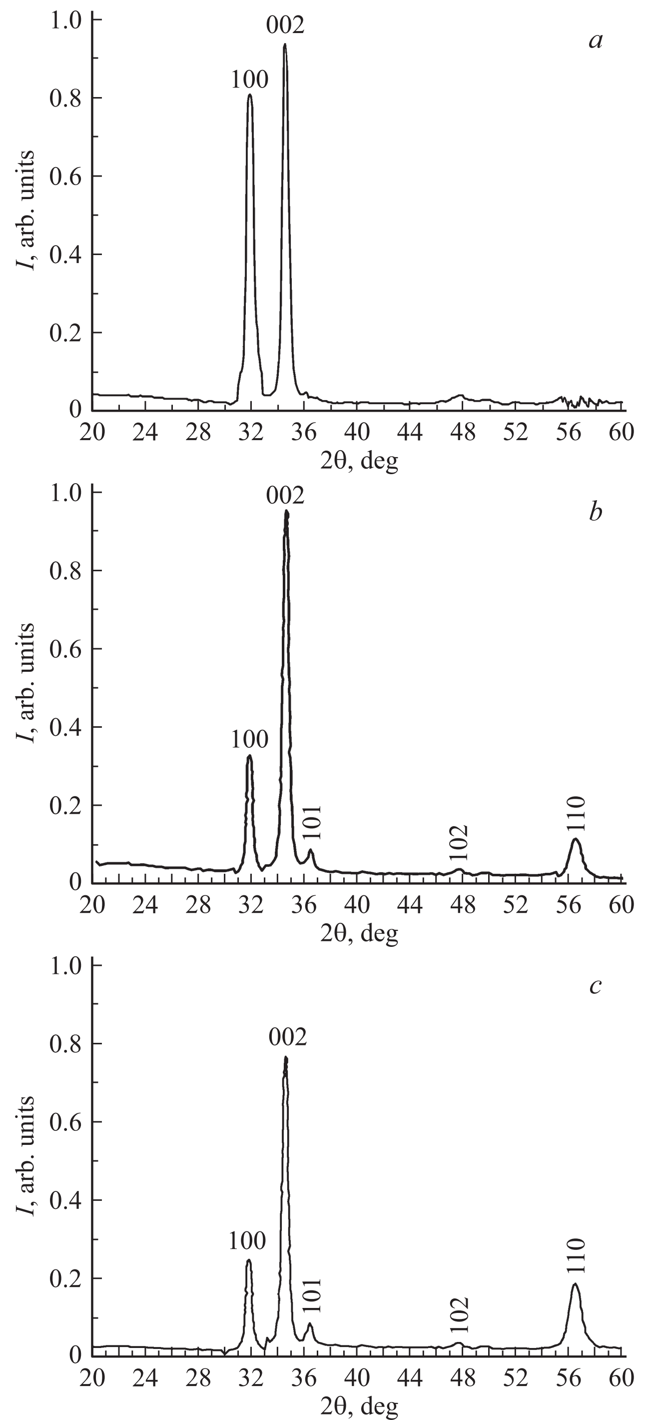

Figure 1. *a* — Diffraction pattern of the thin ZnO film in ZnO–quartz structures; *b* — X-ray diffraction pattern of the polycrystalline zinc oxide film synthesized on a preheated $LiTaO_3$ substrate; *c* — X-ray diffraction pattern of the polycrystalline zinc oxide film synthesized on a cold $LiTaO_3$ substrate.

the diffraction patterns corresponding to a film synthesized on a quartz substrate and on a preheated $LiTaO_3$ substrate remained the same. In the case of synthesis of a zinc oxide film on a cold $LiTaO_3$ substrate, the intensity of peak (002) decreased by 15% relative to the corresponding reflection intensity for a film synthesized on hot $LiTaO_3$ or quartz substrates. Low-intensity reflection (101) in the vicinity of 36° in the diffraction pattern of a film synthesized on a quartz substrate is shifted by 1.3° towards larger angles in the diffraction patterns of ZnO films synthesized on a ferroelectric $LiTaO_3$ substrate, and its intensity increases by a factor of 2 and 3.6 in the case of synthesis on heated and cold $LiTaO_3$ substrates, respectively. Reflection (110), which is not found in the diffraction pattern for a ZnO film formed on a quartz substrate, is seen in the vicinity of 56° in the diffraction patterns of ZnO films formed on $LiTaO_3$ substrates. The intensity of this peak increases when a zinc oxide film grows on a cold substrate: it is 1.8 times higher than the corresponding intensity for a ZnO film formed on a preheated lithium tantalate substrate.

The results of comparison of literature data on diffraction patterns for zinc oxide films synthesized by magnetron sputtering of a ZnO target jcite14-18 with the results of X-ray diffraction analysis of zinc oxide films synthesized by pulsed laser ablation on hot and cold lithium tantalate substrates indicate that the values of intensity of reflections (100) and (002) agree closely. In addition, the angular positions of reflections (100) and (002) for all the synthesized zinc oxide films correlate well with literature data [15–18]. A joint analysis of the diffraction patterns for a zinc oxide film synthesized by pulsed laser ablation of a high-purity target of pressed ZnO powder and the diffraction patterns corresponding to magnetron sputtering of a ZnO target [4,14–16] revealed that diffraction maxima (100), (101), (102), and (110) were lacking in the X-ray diffraction patterns of samples produced by magnetron sputtering.

The film surface roughness was examined with a Solver PRO scanning probe microscope (NT-MDT), and it was found that films synthesized by laser ablation both on a quartz substrate and on a $LiTaO_3$ substrate had a high degree of structural perfection. The roughness of a ZnO film on a quartz substrate did not exceed 80.0 nm, and the roughness of a ZnO film formed on a ferroelectric $LiTaO_3$ substrate did not exceed 97.0 nm.

The spectral dependences of the photoconduction current (Fig. 2) were examined to reveal the presence of traps, which are both electrically and optically active, in ZnO films and to estimate the activation energy and the frequency factor. The setup discussed in [9] was used to study the photoconduction processes. This setup included a Keithley 6487 picoammeter/voltage source and a spectrometric module comprised of a radiation source (xenon lamp with a quartz condenser) and an MDR-41 monochromator. The range of measured currents was 0.01 nA–20 μA. Measurements were performed at room temperature. Scanning over the wavelength in the 300–800 nm spectral bands

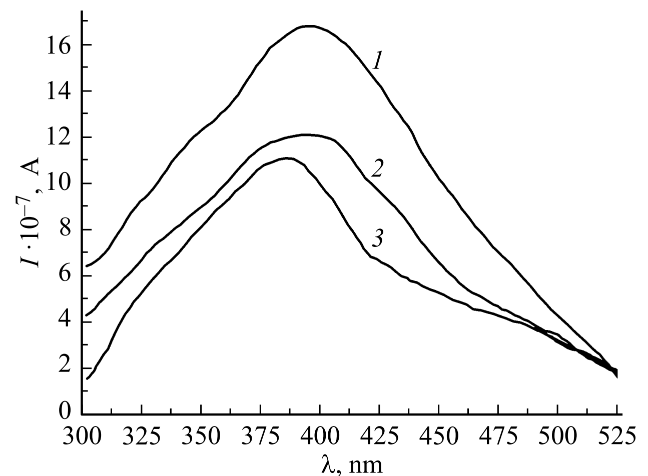

Figure 2. Spectral dependences of the photoconduction current for ZnO–$LiTaO_3$ and ZnO–quartz structures: *1* — ZnO deposited onto a heated $LiTaO_3$ substrate; *2* — ZnO deposited onto a cold $LiTaO_3$ substrate; *3* — ZnO deposited onto a quartz substrate.

was performed pointwise at a rate of 5.0 nm/s. The time of current signal accumulation at each point was set to 10.0 s to exclude the influence of transient currents on the spectral photoconduction profiles. Aquadag electrodes were deposited onto the ends of ZnO strips. Measurements were performed in the planar photoconductive sensor topology.

The spectral dependences of the photoconduction current of the studied structures are presented in Fig. 2: curve *1* corresponds to the photocurrent measured in a ZnO film deposited onto a hot lithium tantalate substrate, curve *2* represents the photocurrent measured in a ZnO film deposited onto a cold lithium tantalate substrate, and curve *3* corresponds to the photocurrent in a film deposited onto a quartz wafer. The spectral dependence of the photocurrent measured in a zinc oxide film formed on a hot $LiTaO_3$ substrate is asymmetric relative to its maximum and bell-shaped: the photocurrent build-up rate is higher than the fall rate. The maximum current is 16.7 μA and corresponds to 394 nm. Having passed through its maximum, the spectral dependence of the photocurrent develops a long tail that decays in the long-wavelength region extending from 400 to 525 nm.

The spectral dependence of the photocurrent for a ZnO film formed on a quartz substrate is also complex in shape and is divisible into several regions. The photocurrent build-up region contains two sublinear sections with widely different current build-up rates: the rate in the 300–320 nm spectral band is 2.3 times higher than the one in the 325–375 nm band. The maximum photocurrent values are located in the 377–390 nm spectral band, and the peak of the photoconduction current (1.08 μA) is at 385 nm. This behavior of the photoconduction current may be attributed to the presence of several types of optically active traps in a ZnO film on quartz that have significantly different densities and activation energies and become involved in

the photoconduction process in the course of scanning over the spectrum.

Spectral dependences of the photocurrent induced by non-equilibrium photogeneration of carriers in a zinc oxide layer and its subsequent transport between electrodes are characterized by the Fredholm integral equation of the first kind. As is known, determining a solution to the Fredholm integral equation of the first kind is a Hadamard ill-posed problem. The Tikhonov–Lavrentiev regularization method is one of the techniques used to solve ill-posed problems. Within this context, we solved the Fredholm equation of the first kind (characterizing the processes of non-equilibrium photogeneration and transport of carriers) using the regularization method with account for the presence of random and systematic errors in input data in order to reconstruct the distribution of traps over activation energy $G(E)$. Distributions $G(E)$ of traps over activation energy in ZnO formed on the surface of a quartz wafer, a preheated lithium tantalate wafer, and a lithium tantalate wafer without preheating were determined by solving the problem numerically. Non-equilibrium photostimulated carriers in a zinc oxide layer formed on the surface of a quartz wafer are generated from monoenergetic deep traps. Their activation energy and frequency factor are listed in Table 1.

Non-equilibrium photostimulated carriers in a zinc oxide layer synthesized on the surface of a preheated lithium tantalate wafer are also generated from monoenergetic deep traps. The corresponding values of activation energy and frequency factor are listed in Table 2.

Non-equilibrium photostimulated carriers in a zinc oxide layer formed on the surface of a lithium tantalate wafer without preheating are again generated from monoenergetic deep traps. Their activation energy and frequency factor are listed in Table 3.

According to literature data, traps with such activation energies are likely to be oxygen or zinc vacancies that are present in zinc oxide [15,16,18]. As is known, oxygen vacancies in zinc oxide may assume three different charge states: neutral, singly ionized, and doubly ionized. Singly ionized oxygen vacancies have activation energies of 0.93, 0.96, 1.82, and 1.84 eV. Doubly ionized oxygen vacancies have activation energies of 0.98, 2.27, 2.58, 2.9, and 3.1 eV. Donors [15–18] are also involved in the processes of photostimulated generation of non-equilibrium carriers. Owing to the involvement of this type of traps in photostimulated processes, sequential transfer of energy occurs in photoionization.

Thus, deep traps with an activation energy of 3.28, 3.27, 3.19, or 3.18 eV, which are exclusive to zinc oxide layers deposited onto the surface of lithium tantalate, contribute to the photoconduction processes in such layers. Deep traps involved in the transport of photostimulated carriers in zinc oxide deposited onto a hot lithium tantalate substrate have an activation energy of 3.28 and 3.19 eV. Deep traps for zinc oxide formed on a cold lithium tantalate substrate have an activation energy of 3.27 and 3.18 eV. The 0.1 eV energy difference is likely to be attributable

Table 1. Activation energy and frequency factor for a zinc oxide layer formed on the surface of quartz wafer

№	Activation energy, eV	Frequency factor, s^{-1}
1	3.1	$2.3 \cdot 10^{-7}$
2	3.0	$5.8 \cdot 10^{-7}$
3	2.9	$7.1 \cdot 10^{-5}$
4	2.55	$4.3 \cdot 10^{-8}$
5	2.36	$2.2 \cdot 10^{-8}$
6	1.95	$4.5 \cdot 10^{-7}$
7	1.82	$8.2 \cdot 10^{-7}$
8	1.23	$1.4 \cdot 10^{-8}$
9	0.98	$3.2 \cdot 10^{-7}$
10	0.96	$3.6 \cdot 10^{-8}$
11	0.93	$7.5 \cdot 10^{-8}$
12	0.9	$3.6 \cdot 10^{-8}$
13	0.87	$2.6 \cdot 10^{-7}$

Table 2. Activation energy and frequency factor for a zinc oxide layer formed on the surface of a preheated lithium tantalate wafer

№	Activation energy, eV	Frequency factor, s^{-1}
1	3.27	$4.3 \cdot 10^{-7}$
2	3.19	$5.7 \cdot 10^{-7}$
3	2.9	$1.1 \cdot 10^{-5}$
4	2.58	$3.3 \cdot 10^{-8}$
5	2.27	$6.2 \cdot 10^{-8}$
6	1.97	$2.5 \cdot 10^{-7}$
7	1.89	$7.2 \cdot 10^{-7}$
8	1.84	$3.4 \cdot 10^{-8}$
9	0.98	$6.2 \cdot 10^{-8}$
10	0.96	$1.5 \cdot 10^{-8}$
11	0.93	$5.2 \cdot 10^{-8}$
12	0.74	$1.7 \cdot 10^{-7}$
13	0.65	$4.3 \cdot 10^{-7}$

Table 3. Activation energy and frequency factor for a zinc oxide layer formed on the surface of a lithium tantalate wafer without preheating

№	Activation energy, eV	Frequency factor, s^{-1}
1	3.28	$3.3 \cdot 10^{-6}$
2	3.18	$4.3 \cdot 10^{-6}$
3	2.9	$3.1 \cdot 10^{-5}$
4	2.67	$4.3 \cdot 10^{-7}$
5	2.58	$5.2 \cdot 10^{-6}$
6	2.27	$8.1 \cdot 10^{-6}$
7	1.93	$2.2 \cdot 10^{-7}$
8	1.84	$8.4 \cdot 10^{-6}$
9	0.98	$5.2 \cdot 10^{-8}$
10	0.96	$3.5 \cdot 10^{-8}$
11	0.93	$1.2 \cdot 10^{-8}$
12	0.75	$3.7 \cdot 10^{-6}$
13	0.68	$2.3 \cdot 10^{-7}$

to the morphology of zinc oxide, which depends on the deposition conditions (substrate temperature). These deep traps involved in the generation of non-equilibrium carriers and in current transport have a frequency factor of $\sim 10^{-6}\,c^{-1}$. This suggests that they are located in ZnO at the semiconductor−ferroelectric interface. In addition, the energy of UV and visible quanta was chosen to be definitely lower than the semiconductor−ferroelectric potential barrier. Therefore, the over-barrier mechanisms of current transport in photostimulated generation of non-equilibrium carriers in the semiconductor−ferroelectric structure may be neglected.

4. Conclusion

The method of pulsed laser ablation of a target (made of extra-pure ZnO powder) with a DPSS laser operated in the giant-pulse mode makes it possible to create thin ZnO films with a high degree of structural perfection on the surface of lithium tantalate. This is evidenced by the presence of intense reflections (001) and (002) in the diffraction patterns of the films under study.

Singly and doubly ionized oxygen vacancies were found to be present in all the studied samples. Deep traps localized at the semiconductor−ferroelectric interface were found in the samples of zinc oxide formed on the surface of lithium tantalate.

The combination of structural and photovoltaic properties of $ZnO-LiTaO_3$ structures makes them suitable for the design of planar photovoltaic, acoustoelectronic, and optoacoustic devices operating in UV and visible ranges.

Funding

This study was supported in part by the Ministry of Science and Higher Education of the Russian Federation (project „State Assignment“, grant No. FSEE-2020-0005).

Conflict of interest

The authors declare that they have no conflict of interest.

References

[1] W.Z. Xu, Z.Z. Ye, Y.J. Zeng, L.P. Zhu, B.H. Zhao, L. Jiang, J.G. Lu, H.P. He, S.B. Zhang. Appl. Phys. Lett., **88**, 173506 (2006).
[2] C.L. Wei, Y.E. Chen, C.C. Cheng. Thin Sol. Films, **518**, 3059 (2010).
[3] Y.K. Chembo, D. Brunner, M. Jacquot, L. Largerl. Rev. Mod. Phys., **91** (3), 035006 (2019).
[4] V.A. Krivchenko, D.V. Lopaev, V.V. Pashchenko, V.G. Pirogov, A.T. Rakhimov, N.V. Suetin, A.S. Trifonov. Tech. Phys., **53** (8), 1065 (2008).
[5] T.V. Blank, Yu.A. Gol'dberg. Semiconductors, **37** (9), 999 (2003).
[6] Zh. Wen, Ch. Li, D. Wu, A. Li, N. Ming. Nature Materials, **12**, 617 (2013).
[7] L.V. Grigor'ev, A.A. Semenov, Ya.B. Egorova, N.A. Bykov, A.A. Nikitin. Opt. Spectrosc., **127** (12), 1080 (2019).
[8] L.V. Grigoryev, A.A. Semenov, I.A. Morozov, N.S. Zhuravlev, A.A. Nikitin. Semiconductors, **54** (3), 285 (2020).
[9] L.V. Grigoryev, A.F. Kraycko, A.V. Mikhailov, V.G. Nefedov, O.V. Shakin. Adv. Mater., Proc. Int. Conf. on „Physics and Mechanics of New Materials and their Applications“, PHENMA-17, v. 207, chap. 19, p. 239 (2017).
[10] O.G. Vendik, Yu.N. Gorin, V.F. Popov. *Korpuskulyarno-fotonnaya tekhnologiya* (M., Vysshaya Shkola, 1984) (in Russian).
[11] W. Prellier, A. Fouchet, B. Mercey, Ch. Simon, B. Raveau. Appl. Phys. Lett., **82**, 3490 (2003).
[12] S. Hermann, T. Dezhindar, H. Harder, R. Brendel. J. Appl. Phys., **108**, 114514 (2010).
[13] A.A. Rusakov. *Rentgenografiya metallov* (M., Atomizdat, 1977) (in Russian).
[14] P. Narin, E. Kutlu, G. Atmaca, A. Atilgan, A. Yildiz, S. Lisesivdin. Optik, **168**, 86 (2018).
[15] U. Helmensonn, M. Latemann, J. Bohlmark, A.P. Ehiasarian, J.T. Gudmudsson. Thin Sol. Films, **513** (1−2), 1 (2006).
[17] B.D. Yao, V.F. Chang, F. Wang. Appl. Phys. Lett., **81**, 757 (2002).
[18] D.M. Bagnal, Z. Chen, T. Yao. Appl. Phys. Lett., **73**, 1038 (1998).